

## Research Paper

# Cuboidal tethered cyclodextrin frameworks tailored for hemostasis and injured vessel targeting

Yaping He<sup>1,2</sup>, Jian Xu<sup>1,2</sup>, Xian Sun<sup>1,2</sup>, Xiaohong Ren<sup>1</sup>, Abi Maharjan<sup>1,2</sup>, Peter York<sup>3</sup>, Yong Su<sup>4</sup>✉, Haiyan Li<sup>1,2</sup>✉, Jiwen Zhang<sup>1,2</sup>✉

1. Center for Drug Delivery Systems, Shanghai Institute of Materia Medica, Chinese Academy of Sciences, 501 Haike Road, Shanghai 201203, China
2. University of Chinese Academy of Sciences, Beijing 100049, China
3. Institute of Pharmaceutical Innovation, University of Bradford, Bradford, West Yorkshire BD7 1DP, United Kingdom
4. Shanghai Fudan-zhangjiang Bio-Pharmaceutical Co., Ltd., Shanghai 201210, China

✉ Corresponding authors: E-mail: jwzhang@simm.ac.cn; ysu@fd-zj.com; lihaiyan821005@163.com

© Ivyspring International Publisher. This is an open access article distributed under the terms of the Creative Commons Attribution (CC BY-NC) license (<https://creativecommons.org/licenses/by-nc/4.0/>). See <http://ivyspring.com/terms> for full terms and conditions.

Received: 2018.11.01; Accepted: 2019.02.13; Published: 2019.04.13

## Abstract

**Rationale:** Targeted delivery of therapeutic drugs or imaging agents to injured blood vessels via nanocarriers is likely to be dependent on the particle shape, yet cubic nanoparticle carriers have not been reported for vascular targeting. Here, we demonstrate that cuboidal cyclodextrin frameworks possess superior hemostasis effect and injured vessels targeting compared with spherical counterpart.

**Methods:** Cuboidal and biocompatible  $\gamma$ -cyclodextrin metal-organic frameworks (CD-MOFs) are synthesized, tethered via crosslinking and surface modification with GRGDS peptide (GS5-MOFs). The specific interactions of cubic GS5-MOF nanoparticles with activated platelets were investigated by in vitro platelet aggregation assay and atomic force microscopy measurements (AFM). The hemostatic capacity and injured vessel targeting efficacy were evaluated in vivo.

**Results:** Cuboidal GS5-MOF nanoparticles exhibit enhanced adhesion and aggregation with activated platelets in vitro under static condition and a physiologically relevant flow environment. The cubic GS5-MOF nanoparticles show efficient hemostatic effects with bleeding time and blood loss decrease of 90% and strong injured vessel targeting in vivo, markedly superior to spherical  $\gamma$ -CD nanosponges with the same chemical composition.

**Conclusions:** These results clearly highlight the contribution of the cuboidal shape of GS5-MOFs to the enhanced aggregation of activated platelets and high targeting to damaged vessels. The cuboidal nanoparticle system provides an innovative delivery platform for the treatment and diagnosis of vascular diseases.

Key words: cuboidal cyclodextrin frameworks; shape control; activated platelets; hemostasis; injured vessel targeting

## Introduction

Vascular diseases such as uncontrolled bleeding, myocardial infarction and stroke are major causes of morbidities and mortalities throughout the world. Targeted delivery of therapeutic drugs and imaging agents for vascular disease therapy (such as hemorrhage, thrombosis and atherosclerosis) remains as still great challenges due to the complex hemodynamics, dynamic changes of lesions and rapid

clearance of conventional spherical drug carrier particles in the blood circulation system [1-3]. The physical properties of nanoparticles, especially the shape and structure, play important roles in the fate and biofunction of carriers [4,5]. It has been reported that filomicelles have much longer circulation time than spherical counterparts [4]. Cylindrical nanoparticles (NPs), such as mesoporous silica

nanorods and calcium phosphate nanorods, were shown to exhibit superior transport and trafficking capability in mucus compared to corresponding nanospheres [5]. Therefore, the introduction of carriers with controlled nonspherical geometries provides new possibilities to enhance vascular targeting by improving the ability of carriers to navigate physiological flow patterns, evade biological clearance, and facilitate adhesion to injured vascular surfaces.

For excessive blood loss, platelets and coagulation factors commonly transfused in the clinic to halt uncontrollable bleeding are greatly limited by their low availability [6-8], high cost, short shelf life, and immunological side effects [9-11]. Consequently, there is an unmet need for developing hemostats to halt bleeding efficiently and selectively at the vascular injury site. As the “first responders” during the wounding process, platelets have an innate ability to migrate to the impaired vascular wall and specifically target and aggregate at the injury site, forming a platelet plug to stem initial blood loss. Therefore, synthetic intravenous hemostatic materials that can mimic, amplify and leverage various biochemical or mechanistic components of platelets have been studied to target vascular injuries and staunch bleeding [12-16]. Accordingly, several platelet-like moieties, including full-length fibrinogen, fibrinogen-derived Arg-Gly-Asp (RGD) peptides and platelet surface glycoproteins, have been designed to decorate liposomes, albumin microparticles, polymer nanoparticles and even erythrocytes to promote platelet adhesion or aggregation [17-21]. It was demonstrated that liposomes only modified with RGD peptide could target and bind to activated platelets [22,23]. Furthermore, platelet-like nanoparticles (PLNs) surface decorated with collagen- and von Willebrand factor-binding peptides combined with a fibrinogen-mimetic peptide (RGD) could mimic the natural platelet's shape and elasticity showing synergistic hemostatic efficacy in a mouse tail amputation model [24].

Hemostatic efficiency, especially the ability to promote the aggregation of activated platelets, is highly dependent on the surface biological functionalities and physico-mechanical properties (size, shape and flexibility) of the particles [24-26]. In particular, the shape of synthetic particles not only plays important roles in their dynamic margination to the wall under flow conditions, but also influences the adhesive and aggregatory biological interactions with activated platelets. Anselmo et al. demonstrated that elastic PLNs could exhibit enhanced surface-binding compared to spherical and rigid discoidal counterparts [24]. Brown et al. designed deformable

platelet-like particles (PLPs) by coating ultrasoft microgels with variable domain-like recognition motifs (sdFv) exhibiting high specificity for fibrin. They found that PLPs could augment clotting under physiological flow conditions *in vitro* and lower bleeding time *in vivo* in a rat traumatic injury model [27]. Particles with anisotropic shapes (e.g., spheroids, ellipsoids, rods) were demonstrated to undergo enhanced adhesion in a physiologically relevant flow environment compared with spherical counterparts [19,26,28]. In addition, particle geometry can influence the ability of carriers to evade *in vivo* clearance and extend circulation time [29]. Therefore, controlling the carrier shape offers opportunities to overcome biological barriers and improve therapeutic effects to vascular diseases. Whilst studies to date have focused on spherical carrier particles, no studies have been reported on using cubic particles for targeted hemostasis and vascular disease treatment.

As an emerging category of multifunctional materials, metal-organic frameworks (MOFs), also known as porous coordination polymers, built from metal ions/clusters and organic linkers via coordination bonds have attracted much attention in biomedicine [30,31]. Compared with other conventional nanomaterials, nanoscale MOFs possess advantages such as superior structures, component tenability and well-shaped geometries [32-34]. Thus, MOFs are attractive materials for effective hemostasis and *in vivo* targeting of vascular injuries. CD-MOFs have regular cubic shape and good chemical modification capabilities, based on our previous research [35], we hypothesized that cuboidal CD-MOF nanoparticles conjugated with Gly-Arg-Gly-Asp-Ser (GRGDS) peptide would be better suited than their spherical counterparts for efficient hemostasis and wound site targeting by enhancing interplatelet interactions and aggregation. To test this hypothesis, biocompatible CD-MOF nanoparticles with an ordered cuboidal architecture were synthesized, tethered via ester-bond crosslinking (CL-MOFs), and surface modified with GRGDS peptide (GS5-MOFs). To elucidate the influences of shape on hemostatic efficacy, corresponding spherical nanoparticles, namely,  $\gamma$ -cyclodextrin nanosponges (CD-NS) with identical chemical compositions and surface charge to CL-MOFs were synthesized by the interfacial condensation method [36,37]. The specific interactions of cubic GS5-MOF nanoparticles with activated platelets were investigated by an *in vitro* platelet aggregation assay and AFM. Subsequently, *in vivo* studies were executed to validate the hemostatic efficiency of the GS5-MOF nanoparticles in a mouse tail transection model and a rat femoral artery injury

model. The in vivo targeting by GS5-MOF nanoparticles to activated platelets at damaged blood vessels in a mouse tail transection bleeding model and a mouse mesenteric thrombosis model was also examined.

## Materials and methods

### Materials

$\gamma$ -CD was purchased from MaxDragon Biochem Ltd. (Guangzhou, Guangdong, China). DPC (99%) was supplied by Aladdin Reagent Co., Ltd. (Shanghai, China). Potassium hydroxide (KOH), polyethylene glycol 20000 (PEG 20000), *N,N'*-carbonyldiimidazole (CDI), triethylamine (TEA), 4-dimethylaminopyridine (DMAP), *N,N*-dimethylformamide (DMF), methanol, ethanol, acetonitrile, acetone and other reagents of analytical grade were purchased from Sinopharm Chemical Reagent Co., Ltd. (Shanghai, China). Water was purified by a Milli-Q system (Millipore, Billerica, Massachusetts, USA). The linear fibrinogen-mimetic peptide GRGDS was synthesized by China Peptides Co., Ltd. (Shanghai, China). 1-(3-Dimethylamino-propyl)-3-ethylcarbodiimide (EDC) was purchased from Tokyo Chemical Industry Co., Ltd. (Shanghai, China). Adenosine 5'-diphosphate (ADP), bovine serum albumin (BSA), collagen, aqueous phosphate solution (49%-51%) and 2,2,2-trifluoroethanol (TFE) were purchased from Sigma-Aldrich (St. Louis, Missouri, USA). The fluorescent dye of carboxyfluorescein diacetate succinimidyl ester (CFDA-SE) was provided by Beyotime Biotechnology (Shanghai, China). Cyanine 5 NHS ester (Cy5) was supplied by Xi'an Ruixi Biological Technology Co., Ltd. (Xi'an, Shanxi, China). RPMI-1640 medium was purchased from Corning Inc. (Corning, New York, USA). Penicillin, streptomycin, acetic acid, polysorbate 80 (Tween 80) and dimethyl sulfoxide (DMSO) were obtained from Sigma-Aldrich (St. Louis, Missouri, USA). All reagents were commercially available and used as received.

### Synthesis of CL-MOF nanoparticles with a cuboidal shape

Nanosized CD-MOF crystals were synthesized according to our previously reported method [38]. The CL-MOF nanoparticles were synthesized directly using CD-MOF crystals [39]. The harvested crystals of CD-MOFs (60 mM) were incubated in DMF with DPC (360 mM) at a 1:6 molar ratio (CD: DPC). Then, 450  $\mu$ L of TEA was added as a catalyst to speed up the reaction. The particles were stirred at 80 °C for 24 h. When the condensation polymerization reaction was complete, the reaction mixture was cooled to room temperature and a 2-fold volume of ethanol was added to quench the reaction. The CL-MOF

precipitates were then washed with 50% ethanol, water and acetone and finally dried under vacuum at 40 °C overnight.

### Synthesis of CD-NS with a spherical shape

The interfacial condensation method was employed to synthesize spherical CD-NS with CDI as an agent to crosslink the hydroxyl groups in  $\gamma$ -CD [36]. In detail, 3.891 g of  $\gamma$ -CD (3.00 mmol) was completely dissolved in 20 mL of a 0.1 M aqueous solution of KOH ultrasonically. The aqueous solution was filtered through a 0.8  $\mu$ m hydrophilic filter membrane. Next, 1.297 g of CDI (8.00 mmol) was dissolved in 20 mL of  $\text{CH}_2\text{Cl}_2$  to obtain an organic solution of CDI. The alkaline  $\gamma$ -CD solution was then added to the organic CDI solution under continuous magnetic stirring (600 rpm) at room temperature. After reaction for 30 min, the precipitate was washed with absolute ethanol and then deionized water and centrifuged at 4000 rpm for 5 min after each wash. The product was collected and dried by lyophilization to obtain CD-NS.

### RGD biofunctionalization

Stable linking of GRGDS peptides to the surface of CL-MOFs and CD-NS is essential for strong platelet adhesion and aggregation. To provide stable linkages, GRGDS peptide was covalently attached to CL-MOF and CD-NS nanoparticles via a stable covalent ester bond by reacting the surface hydroxyl groups of CL-MOFs and CD-NS with the C-terminus of GRGDS. In detail, CL-MOFs (or CD-NS) and GRGDS were added to a round-bottom flask with DMF as the solvent, and the simple chemical reaction was carried out with heating, stirring and EDC and DMAP as catalysts at 37 °C for 24 h to couple the GRGDS peptide to the surfaces of the CL-MOF nanoparticles (or CD-NS). The product was then washed with methanol and water twice and dried by lyophilization. The GRGDS-modified CL-MOF and CD-NS nanoparticles were named GS5-MOF and GS5-NS, respectively.

Cy5 (excitation maximum: 646 nm; emission maximum: 660 nm) was used to fluorescently label the CL-MOF, GS5-NS and GS5-MOF nanoparticles by reacting the free hydroxyl group (-OH) in CD with the activated carboxyl group (-COOH) in Cy5. Namely, 2.4 mg of Cy5 and 230 mg of CL-MOF (GS5-NS or GS5-MOF) nanoparticles in 5 mL of DMF were stirred for 12 h at 37 °C in the dark.

### Aggregation of GS5-MOFs with activated platelets under dynamic conditions

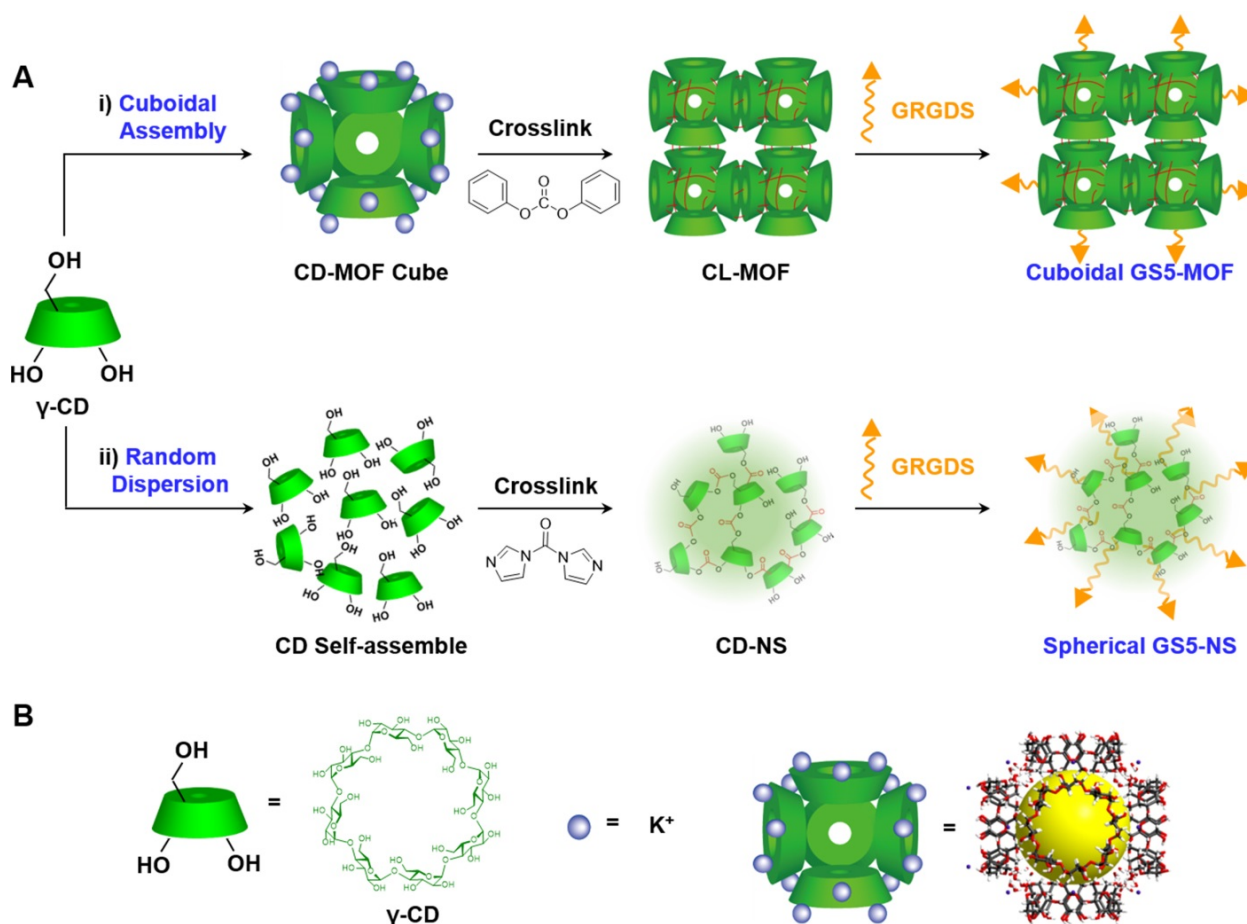
The interaction of nanoparticles with activated platelets in a flow environment was studied using a parallel plate flow chamber (PPFC) (31-010,

GlycoTech, Gaithersburg, Maryland, USA) connected to a programmable pump (Fusion 200, Chemyx, Inc., Stafford, USA) and recirculating loop with silicone tubing, which is appropriate for biomolecular interaction analysis under a dynamic shear flow environment. In the PPFC, by maintaining the Reynold's number in the "laminar" range ( $\sim 10^5$ ), the wall shear stress ( $\tau_w$ ) can be modulated as a function of the flow rate (Q) by the equation (1):

$$\tau_w = \frac{6\mu Q}{bh^2} \quad (1)$$

where  $\mu$  is the fluid viscosity,  $b$  is the width of the PPFC chamber, and  $h$  is the distance between PPFC plates. For our experiments,  $\mu$  was  $0.012 \text{ dyn}\cdot\text{s}\cdot\text{cm}^{-2}$ ,  $b$  was  $1 \text{ cm}$ ,  $h$  was  $0.0127 \text{ cm}$ ,  $b/h$  was  $>20$ , and  $Q$  was controlled by a programmable pump to allow a wall shear stress range of  $5\text{--}55 \text{ dynes}\cdot\text{cm}^{-2}$ , which covered the main range of physiological and pathological shear stresses in blood flow.

Activated platelet-coated and BSA-coated slides were prepared as follows. First, the glass slides were coated with collagen ( $100 \mu\text{g}\cdot\text{mL}^{-1}$ ) and 5% BSA for 12 h at  $4 \text{ }^\circ\text{C}$  and rinsed with  $200 \mu\text{L}$  of PBS to form BSA-coated and collagen-coated adjacent regions. Then,  $100 \mu\text{L}$  of ADP-activated platelets was gently added to the coated regions and incubated at room temperature for 2 h. The prepared slides were rinsed 3 times with  $200 \mu\text{L}$  of PBS to form a layer of activated platelets on the collagen-coated region but not on the BSA-coated region of the slides. The coated slides were vacuum-sealed in the PPFC for subsequent experiments, and the PPFC setup was placed under an inverted fluorescence microscope (Leica TCS-SP8 STED, Wetzlar, Hessen, Germany). Then, Cy5-labeled nanoparticles, at a concentration of  $2 \text{ mg}\cdot\text{mL}^{-1}$ , were allowed to flow through the PPFC in a closed loop over the activated platelet-coated and BSA-coated surfaces under various flow rates to produce different wall shear stresses for 45 min. The slides were imaged at various time points (5, 15, 30, 35, and 45 min)



**Scheme 1.** Schematic synthesis of CL-MOF, GS5-MOF and GS5-NS nanoparticles. (A) Cuboidal CD-MOF nanoparticles were prepared by reacting  $\gamma$ -CDs with KOH. The hydroxyl groups of  $\gamma$ -CDs in CD-MOFs were crosslinked by diphenyl carbonate (DPC) to produce CL-MOF. Finally, activated platelet-targeting peptide, GRGDS, was conjugated on the surfaces of CL-MOF to obtain GS5-MOF nanoparticles. The original cubic shape of the CD-MOFs was retained in both the CL-MOF and GS5-MOF nanoparticles. For comparison, the corresponding spherical CD-NS nanoparticles with similar particle sizes and chemical compositions (tethering  $\gamma$ -CD by ester bond) were also synthesized and modified with GRGDS (GS5-NS). (B) The green cube and purple circle represent  $\gamma$ -CD and KOH, respectively. The highly porous CD-MOF is represented as a  $(\gamma\text{-CD})_6$  cube with a pore diameter of  $1.7 \text{ nm}$  and  $\gamma$ -CD orifices diameter of  $0.78 \text{ nm}$ .

during the flow period using an inverted fluorescence microscope with a 40× objective. Images were collected using Leica software. For image analysis, the surface averaged fluorescence intensities of 10 images per time point per shear stress were analyzed using Image-Pro Plus (Media Cybernetics, Inc., Rockville, Maryland, USA).

### Platelet aggregation under static conditions

#### (i) Fluorescent labeling of rat platelets.

Platelet-rich plasma (PRP) was prepared by centrifugation of freshly collected citrated rat blood at 900 rpm for 15 min at 22 °C. The supernatant, containing platelet-poor plasma (PPP), was removed after centrifuging the PRP at 2500 rpm for 10 min. The obtained platelets were resuspended in HEPES buffer (140 mM NaCl, 3 mM KCl, 0.5 mM MgCl<sub>2</sub>, 5 mM NaHCO<sub>3</sub>, 10 mM glucose, and 10 mM HEPES, pH = 7.4). The reconstituted platelets were then stained with 10 μM CFDA-SE (5 mM stock in DMSO, with the excitation and emission wavelength of 488 nm and 518 nm, respectively) for 40 min at room temperature and centrifuged at 2500 rpm for 10 min. HEPES buffer was removed, and the remaining platelets were resuspended in PPP for further use. **(ii) Platelet aggregation assay.** Five milligrams of nanoparticles was dispersed in 1.0 mL of TFE and 100 μL of the dispersed nanoparticle solution was added to each well of a 24-well plate with coverslips. With the evaporation of TFE, the coverslips in the well can be effectively coated by the nanoparticles. After the TFE had evaporated completely, the wells were washed with PBS three times to remove the free nanoparticles. Then, 100 μL of PRP with CFDA-SE fluorescently labeled platelets was added to each well, and 10 μL of 100 μM ADP as a proaggregatory stimulus or PBS as a control was added. Immediately after the ADP or PBS addition, the 24-well plate was shaken in a shaker at 180 rpm for 1 min. After equilibration for 5 min, plasma and non-aggregated platelets were removed, followed by polyoxymethylene fixation at room temperature for 15 min. After gently washing with PBS two times, the coverslips were inverted on the slide and imaged under a fluorescence microscope (Leica DM 6B, Wetzlar, Hessen, Germany). **(iii) AFM measurements.** The adhesion force between the nanoparticles and the activated platelets was also measured by AFM (FastScan AFM Scanner, Bruker, Karlsruhe, Baden-Wuerttemberg, Germany) [40]. The nanoparticles were first immobilized on a V-shaped triangular silicon cantilever (MLCT-O10, tipless nitride lever, 0.1 N m<sup>-1</sup> spring constant, Bruker, Karlsruhe, Baden-Wuerttemberg, Germany) using a thin layer of epoxy resin. The platelets were coated on the surface of glass slides mediated by collagen.

Multiple force curves for the interactions between the nanoparticle probes and activated platelets were measured in PBS (pH = 7.4) in contact mode in fluid. Force-distance curves were recorded with a tip radius of 80 nm, tip half-angle of 18° and sample Poisson's ratio of 0.3. The data were processed with NanoScope Analysis software (version 1.8) to calculate the adhesion force values.

### In vitro clot formation assay

Citrated anticoagulated whole blood and 80 μL of 0.1 M calcium chloride (CaCl<sub>2</sub>) were mixed in Eppendorf tubes, and nanoparticles dispersed in saline were added to make the final volume to 800 μL, the final concentrations of CL-MOFs and GS5-NS were 20 μg mL<sup>-1</sup>. Then, 60 μL of the samples was deposited into sequential wells on a 96-well plate. Each well was washed with saline solution to halt clotting every 30 s. The liquid was immediately aspirated, and the washing steps were repeated until the wash solution was clear, which indicated complete removal of soluble blood components. Samples were considered clotted when the clot covered the bottom of the well and remained unchanged between time points, and the final clotting time was marked.

### In vivo hemostatic effect

All experiments were performed according to protocols approved by the Institutional Animal Care and Use Committee (IACUC) of Shanghai Institute of Materia Medica, Chinese Academy of Sciences (CAS). **(i) In vivo hemostatic effect in a mouse tail transection model.** GS5-MOF (20 mg·kg<sup>-1</sup> and 40 mg·kg<sup>-1</sup>), CL-MOF (20 mg·kg<sup>-1</sup>) and GS5-NS (20 mg·kg<sup>-1</sup>) nanoparticles in saline solution were injected via the tail vein into healthy male Kunming mice (18-24 g, n = 10, IACUC Application No. 2017-08-ZJW-15, Shanghai Laboratory Animal Center, CAS, Shanghai, China). Five minutes after injection, 0.5 cm long sections of tail from the distill tip were amputated. Bleeding cessation was defined as no observation of bleeding for 20 s. The bleeding time was recorded until the bleeding from the amputated tail stopped. The blood was absorbed by filter paper every 20 s, the filter paper touched the amputated tail lightly to avoid any influence of pressure on bleeding, and the blood loss was assessed by the area of the blood stain using Image-Pro Plus software. **(ii) In vivo hemostatic effect in a rat femoral artery injury model.** Sprague-Dawley rats (SD rats, IACUC Application No. 2018-05-ZJW-18, Shanghai Laboratory Animal Center, CAS, Shanghai, China) were initially anesthetized, then saline, GS5-MOF (14 mg·kg<sup>-1</sup> and 28 mg·kg<sup>-1</sup>), CL-MOF (14 mg·kg<sup>-1</sup>) and

GS5-NS (14 mg·kg<sup>-1</sup>) nanoparticles in saline solution were injected via the tail vein into healthy SD rats (200-240 g, n = 6). The dose of 14 mg·kg<sup>-1</sup> in a rat is equivalent to 20 mg·kg<sup>-1</sup> in a mouse based on relative body surface area. After 5 min of administration, injury at the middle segment of the femoral artery was induced by puncture with a 26-gauge needle [13]. Bleeding cessation was defined as no observation of bleeding for 10 s. The bleeding time was recorded until the bleeding from the injured femoral artery stopped. All the procedures were performed by the same operator blinded to the treatment groups.

### The influences on hemostasis balance

To investigate the influences of GS5-MOF nanoparticles on hemostasis balance, GS5-MOF nanoparticles in saline solution were injected via tail vein into healthy or tail injured male Kunming mice (18-24 g, n = 6) at the dose of 40 mg·kg<sup>-1</sup>. Citrated anticoagulated whole blood was collected at 10 min or 4 h after injection. In addition, the saline and GS5-NS groups were conducted in healthy male Kunming mice and whole blood was collected 10 min after injection. The control group was healthy mice with no injection. Plasma was prepared by centrifugation of freshly collected blood at 3000 rpm for 10 min at 22 °C. The coagulation indicators including prothrombin time (PT), activated partial thromboplastin time (APTT), thrombin time (TT) and fibrinogen content (FIB) were measured by platelet aggregation factor analyzer (LG-PABER-I, Beijing Shidi Scientific Instrument Company, Beijing, China) within 2 h.

### In vivo targeting to activated platelets at vascular injury sites

(i) **Targeting efficiency in a mouse tail transection model evaluated by fluorescence imaging.** The in vivo targeting efficiencies of CL-MOF, GS5-NS and GS5-MOF nanoparticles were examined after intravenous injection of Cy5-labeled nanoparticles (20 mg·kg<sup>-1</sup>) into male BALB/c nude mice (6-8 weeks, 18-20 g, IACUC Application No. 2018-01-ZJW-17, Shanghai Laboratory Animal Center, CAS, Shanghai, China). Five minutes following the injection, the tail was amputated 1.0 cm from the end of tail. Then, at 15 min post-injection, a 1.0 cm long section of the tail from the first amputation was removed and photographed using an in vivo imaging system (IVIS Spectrum, PerkinElmer, Waltham, Massachusetts, USA). The vascular injury-targeting efficiency was evaluated by statistical comparison of the fluorescence intensity in the amputated sections of tail for the CL-MOF, GS5-NS, and GS5-MOF nanoparticles. (ii) **Targeting efficiency in a mouse tail transection model evaluated by microCT**

**imaging.** Ag-loaded samples were synthesized for microCT imaging. First, Ag-loaded CD-MOF (Ag@CD-MOF) nanoparticles were prepared according to the reported method [41], with diffusion of 10 mM AgNO<sub>3</sub> precursor in 600 mg of CD-MOF nanocrystals in acetonitrile for 72 h at room temperature. The suspension was centrifuged, and the precipitate was washed with acetonitrile three times and dried at 40 °C under vacuum for 12 h (Ag@CD-MOFs were characterized completely). Then, Ag-loaded CL-MOF and GS5-MOF (Ag@CL-MOF and Ag@GS5-MOF) nanoparticles were fabricated using the methods described above. The in vivo targeting efficiency of CL-MOF and GS5-MOF nanoparticles was examined after intravenous injection of Ag-loaded nanoparticles (20 mg·kg<sup>-1</sup>) into male Kunming mice (8 weeks, 18-20 g, IACUC Application 2017-08-ZJW-15). Five minutes following the injection, 1.0 cm long fragments of tail were amputated from the distill tip. Then, at 1 h post injection, a 1.0 cm long section of the tail beginning from the site of the first amputation was removed and photographed using a microCT imaging system (Hamamatsu version 2.0.1) at the Shanghai Synchrotron Radiation Facility (SSRF) with a voltage of 80 kV, current of 500 mA, resolution of 26 μm, and distance between the source and object of 12 cm. The distance between the source and detector was maintained at 18 cm. The exposure time was constant at 0.2 s, and the readout time was 0.5 s. A total of 2700 projections were acquired for each 360-degree rotation of sample. The projection was reconstructed by Octopus reconstruction software and then analyzed by Image-Pro Plus software and Amira software (Visage Imaging, Inc., Melbourne, Victoria, Australia). The vascular injury-targeting efficiency was evaluated by a statistical comparison of the gray values in the amputated section of tail with the GS5-MOF and CL-MOF nanoparticles. (iii) **Targeting efficiency in an FeCl<sub>3</sub>-induced mouse mesenteric thrombosis model evaluated by fluorescence imaging.** Male BALB/c nude mice (8 weeks, 18-20 g, IACUC Application No. 2018-01-ZJW-17) were anesthetized with an intraperitoneal injection of pentobarbital sodium (2%, 5 mL·kg<sup>-1</sup>) and placed in the supine position on the lid of a 15 cm tissue culture plate [42]. A midline incision was made through the skin from the xiphoid to lower abdomen, and the middle peritoneum was cut longitudinally. The intestines were exteriorized, and the second branches were used for the thrombosis experiment. Before thrombus was induced, 100 μL of rhodamine B solution (0.5 mg·mL<sup>-1</sup>) was injected via tail vein into mice for the visualization of the process of thrombus formation. A filter paper (2 mm × 4 mm size)

saturated with 12.5% FeCl<sub>3</sub> was directly placed on the mesenteric artery and vein for approximately 5 min to generate vascular injury. Immediately after the initiation of thrombus formation, CL-MOF, GS5-NS and GS5-MOF nanoparticles labeled with Cy5 were injected intravenously (20 mg·kg<sup>-1</sup>). Fluorescence imaging of the thrombus and nanoparticles was performed with a fluorescence imaging system (Olympus IX73, Tokyo, Honshu, Japan).

### Statistical analysis

All experiments were carried out in at least triplicate, and the results are shown as the mean ± SD. A significant difference between two groups was analyzed by Student's t-test and considered significant when  $p < 0.05$  (\*) and highly significant when  $p < 0.01$  (\*\*) and  $p < 0.001$  (\*\*\*).

## Results and Discussion

### Fabrication and functionalization of cuboidal tethered cyclodextrin frameworks

Cuboidal tethered cyclodextrin frameworks were fabricated using cubic CD-MOFs as a template and then crosslinked by ester bonds. The CD-MOFs constructed by  $\gamma$ -CDs together with potassium ions were highly porous (with relatively high surface areas up to 1200 m<sup>2</sup>·g<sup>-1</sup>) and had body-centered cubic extended structures [35]. The  $\gamma$ -CDs in the CD-MOF crystals were further crosslinked with DPC in DMF at 80 °C [39] to obtain CL-MOF nanoparticles, which not only tethered  $\gamma$ -CDs in CD-MOFs to create a cuboidal organization but also improved the stability of the particles in aqueous solution. Spherical CD-NS were also synthesized to have similar particle size, identical zeta potential and chemical composition with CL-MOFs, to enable nanoparticle shape to be the single variable differentiating the tested systems. Careful and controlled functionalization is critical in optimizing the performance of nanoparticles in vivo. In this study, to achieve in vivo targeting and effective hemostasis at vascular injury sites, the fibrinogen-mimetic peptide GRGDS was selected as the functionalization agent since the specific binding of the RGD sequence in fibrinogen to the GPIIb-IIIa receptors on activated platelets is the final pathway for platelet aggregation and plug formation. GRGDS was covalently conjugated onto the surface of CL-MOF and CD-NS nanoparticles via ester bond.

The particle size distributions of the crosslinked and functionalized nanoparticles were characterized by scanning electron microscopy (SEM) and dynamic light scattering (DLS) techniques. As indicated by the SEM images (Figure 1A), nanometer-scale (~200 nm) cubic CL-MOF and GS5-MOF nanoparticles, spherical

GS5-NS were produced. In situ measurements by DLS also revealed a mean diameter of approximately 200 nm (Figure 1B) with a very narrow size distribution, and the average zeta potential of nanoparticles was approximately -25 mV (Table S1). Notably, the cubic morphologies CD-MOF nanocrystals were maintained after crosslinking with DPC and surface modification with GRGDS. The stability in different media (water, saline solution, PBS (pH = 7.4) and serum) indicated high structural integrity of the CL-MOF and CD-NS nanoparticles, with less than 10% free CDs released within seven days (Figures 1C, S1 and S2). The cellular toxicity of the CL-MOF nanoparticles was evaluated on the basis of cell viability using MTT assay in MCF-7, Hela and J774A.1 cell lines. The cell viability remained at almost 100% as the concentrations of CL-MOF and CD-NS nanoparticles increased to 1000  $\mu$ g·mL<sup>-1</sup>, indicating very good cytocompatibility of these nanoparticles (Figures 1D and S3). The typical Fourier transform infrared (FTIR) absorbance peaks for GS5-MOF and GS5-NS nanoparticles located at ~1200, 1540 and 1680 cm<sup>-1</sup> (vibration peak of amide bonds in GRGDS, Figure 1E) and the GRGDS <sup>1</sup>H nuclear magnetic resonance (<sup>1</sup>H NMR) proton signal at  $\delta = 2.7\sim 2.9$  ppm (Figures S5 and S6) confirmed the successful modification of GRGDS on the surface of the CL-MOF and CD-NS nanoparticles.

### In vitro adhesion and aggregation of GS5-MOFs with activated platelets under shear stresses

The platelet-aggregating ability of the cuboidal and spherical nanoparticles with/without GRGDS modification was assessed in vitro in a PPFC setup (Figure S9). To study the interaction of the nanoparticles with activated platelets, PRP was incubated in the presence of ADP, which facilitated the transition of quiescent platelets to activated platelets. Adjacent regions in glass slides were coated with BSA (negative control surface) and collagen, and a layer of activated platelets was formed on the collagen-coated region but not on the BSA-coated region. In the PPFC set up, red fluorescent CL-MOF, cubic GS5-MOF and spherical GS5-NS nanoparticles flowed over these coated glass slides at both physiological and pathological wall shear stresses of 5-55 dynes·cm<sup>-2</sup>. The adhesion and aggregation of targeted (GS5-MOF, GS5-NS) and nontargeted (CL-MOF) nanoparticles to both targeted (activated platelet surface) and nontargeted surfaces (BSA surface) were imaged and quantified. GRGDS-modified nanoparticles should bind specifically to the activated platelet surface. Figure 2A shows a quantitative analysis of the surface averaged

fluorescence intensity from aggregates of various nanoparticles, and **Figure 2B** shows a representative set of fluorescence images taken at 45 min. Unmodified CL-MOF nanoparticles had minimal adhesion on the activated platelet surface. Furthermore, minimal adhesion of GS5-MOF nanoparticles occurred on the nontargeted BSA surface at all shear values. In comparison, GS5-MOFs showed significantly enhanced binding on the activated platelet surface (larger fluorescent “patch” areas) as a result of the specific strong interaction of GRGDS on the surface of nanoparticles with integrin GPIIb-IIIa receptors on the activated platelets. Additionally, a stronger interaction of GS5-MOF nanoparticles with activated platelets was found at the highest shear stress of 55 dynes·cm<sup>-2</sup> than that at lower shear stress values, while minimal adhesion was found on BSA-coated surfaces irrespective of the shear stresses. Importantly, the shape of particles (cuboidal and spherical) also significantly impacted

the adhesion of GRGDS-modified nanoparticles on activated platelet-covered surfaces. The cubic GS5-MOFs covered a larger activated platelet-coated region and showed higher fluorescence intensity than their spherical counterparts (**Figure 2**). The observed enhanced adhesion of GS5-MOF nanoparticles with activated platelets can be attributed to one or other of the two following explanations. Firstly, the unique cubic shape of GS5-MOF increases the contact surface area and collision frequency with activated platelets. Secondly, the  $\gamma$ -CDs in GS5-MOF are ordered and directional which enables full exposure of the GRGDS peptides on the GS5-MOF surface and thus complete targeting capacity is achieved. Therefore, the cuboidal GS5-MOFs showed stronger interaction with integrin GPIIb-IIIa receptors on activated platelets than the spherical GS5-NS. In summary, these in vitro flow experiments demonstrated that cuboidal GS5-MOF nanoparticles could specifically adhere and aggregate to activated platelets at injured vascular sites.

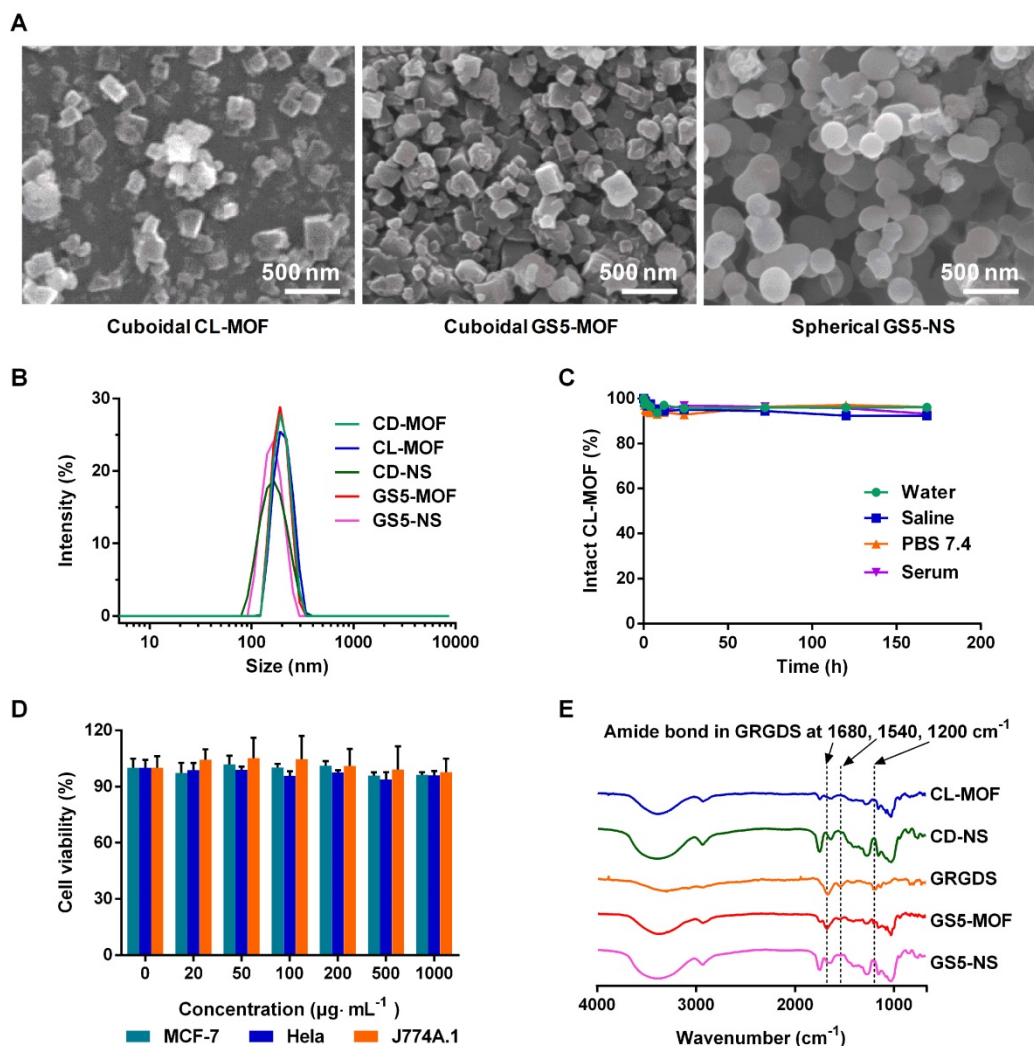


**Figure 1.** Design and characterization of CL-MOF, GS5-MOF and GS5-NS nanoparticles. GS5-MOF nanoparticles are cuboidal carriers with uniform sizes (200 nm), good cytocompatibility and stability. (A) Representative SEM images of CL-MOF, GS5-MOF and GS5-NS nanoparticles. Scale bars = 500 nm. (B) DLS measurements of CD-MOF, CL-MOF, GS5-MOF, CD-NS and GS5-NS nanoparticles. (C) Stability evaluation of CL-MOF nanoparticles in various media. (D) The cytotoxicity of CL-MOF nanoparticles tested in MCF-7, HeLa and J774A.1 cell lines. (E) FTIR analysis of the conjugation of GRGDS with CL-MOF and CD-NS.

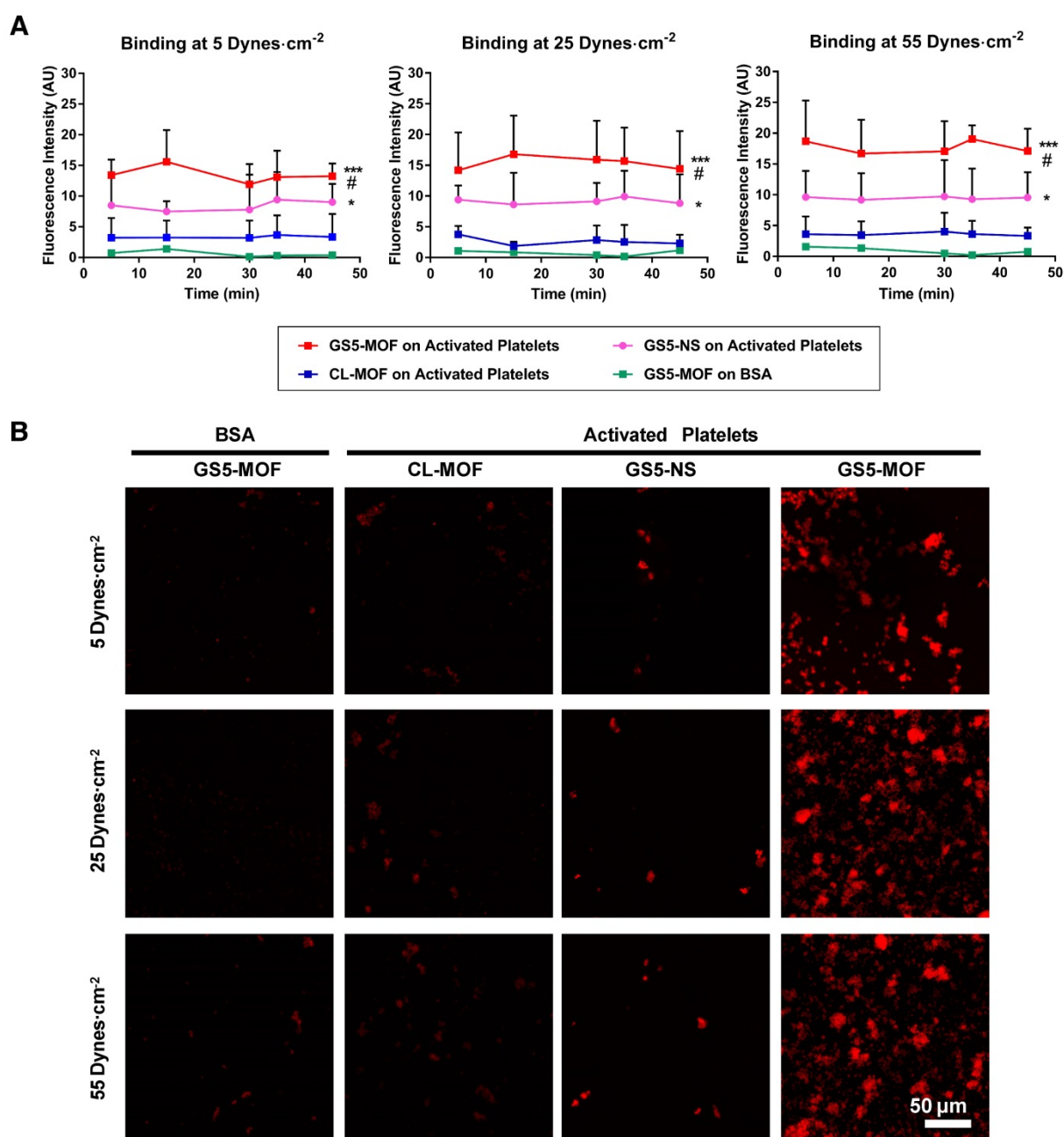


**Figure 2.** In vitro binding of CL-MOF, GS5-NS and GS5-MOF nanoparticles to activated platelet-coated surfaces versus platelet-deficient surfaces under flow conditions. The cubic GS5-MOFs show enhanced binding and aggregation with activated platelets compared to their spherical counterparts. (A) Quantitative surface averaged fluorescence intensity data at different time points. (B) Representative fluorescence microscopy images at 45 min. The large red fluorescent “patch” areas indicate the strong binding of GS5-MOF nanoparticles with the activated platelet-coated surface. GS5-MOF nanoparticles showed specific binding to activated platelet-coated surfaces (filled squares in red) and minimal adhesion to nontargeted control BSA surfaces (filled squares in green), while CL-MOFs without GRGDS modification showed minimal binding to activated platelet-coated surfaces (filled squares in blue). At least 10 images for each condition at each time were acquired for analysis. Scale bar = 50  $\mu\text{m}$ . Values are the mean  $\pm$  SD ( $n = 10$ ). \*Denotes a significant difference compared with the CL-MOF control. \* $p < 0.05$ , \*\*\* $p < 0.001$ . #Denotes a significant difference ( $p < 0.05$ ) between cubic GS5-MOF and spherical GS5-NS groups.

### In vitro activated platelet aggregation under static conditions

Based on the strong adhesion of GS5-MOF nanoparticles to activated platelets observed in the PPFC experiments, the enhanced aggregation of activated platelets by cubic GS5-MOF nanoparticles was cross validated via an in vitro platelet aggregation assay [11]. As evident from the results

(Figures 3B and 3C), there was minimal aggregation of activated platelets onto the unmodified CL-MOF-coated coverslips. Conversely, significantly more aggregation of activated platelets and stronger fluorescence signals were found in the GS5-MOF-covered region than in the CL-MOF-covered region, which indicates an increase in activated platelet aggregation by GS5-MOFs. Consistent with the results from the dynamic PPFC experiment shown in Figure

2, stronger aggregation of activated platelets was found for the cubic GS5-MOF nanoparticles than the spherical GS5-NS particles. It is critical for clinical utility that the nanoparticles specifically bind and promote the aggregation of activated platelets with minor binding to resting platelets and no induction of platelet activation to avoid adverse thrombotic events such as embolism and stroke. As shown in **Figure 3B**, no binding of nonactivated platelets (PBS group) to the GS5-MOF nanoparticles was observed, and the activation of quiescent platelets was not induced by GS5-MOFs without the addition of ADP. Therefore,

GS5-MOF nanoparticles specifically bind and promote the aggregation of activated platelets without binding to quiescent platelets or activating endogenous resting platelets.

High colocalization of Cy5 labeled GS5-MOF nanoparticles (red) with CFDA-SE stained platelets (green) in the presence of ADP was also observed (**Figure 3D**), indicating the presence of both GS5-MOFs and activated platelets in the formed aggregates. Colocalization of the activated platelets and nanoparticles was further quantified using multiple images via Pearson's coefficient (**Figure 3E**).

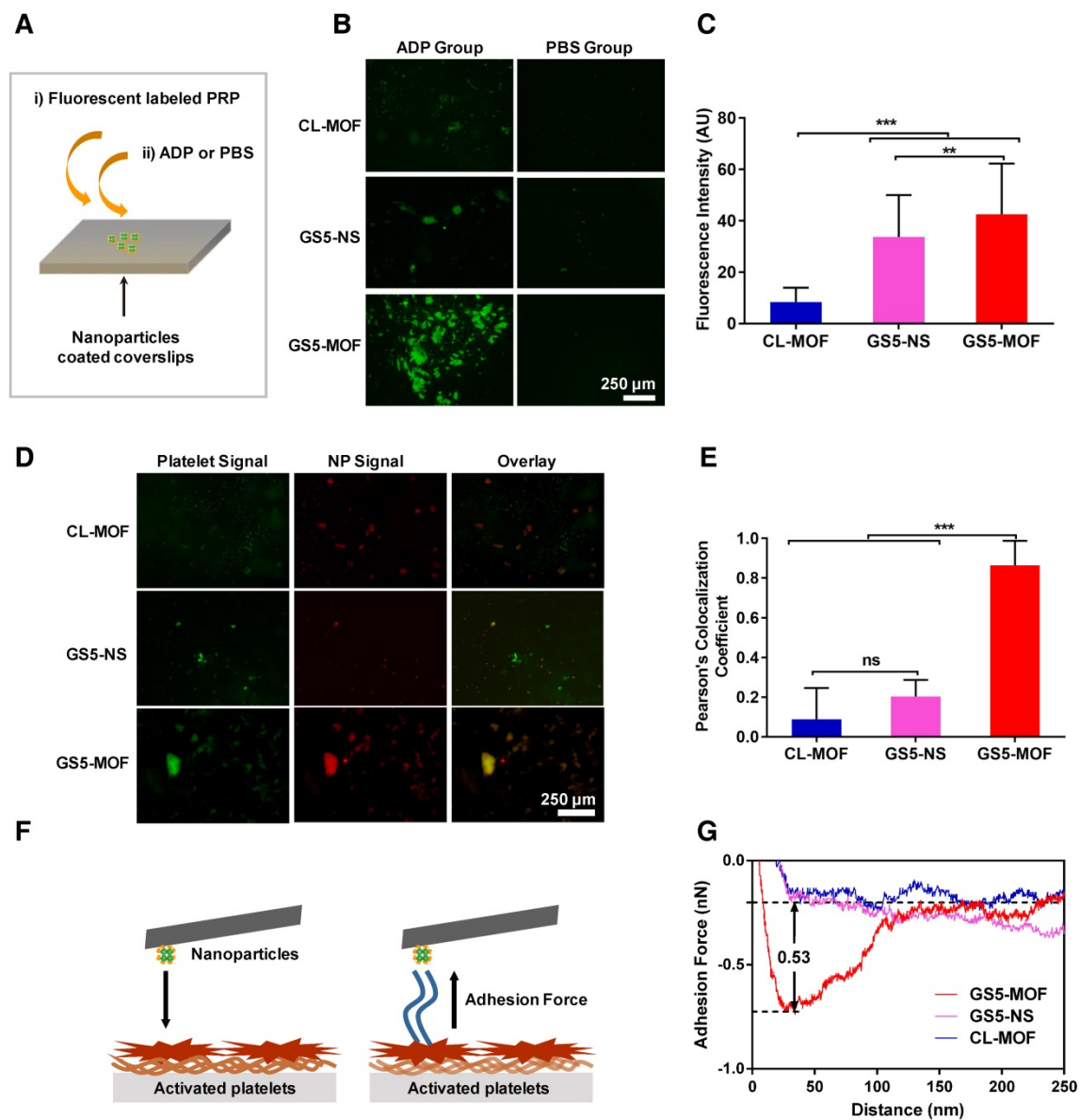


**Figure 3.** In vitro activated platelet aggregation under static conditions. Enhanced activated platelet aggregation and higher colocalization were found with a cuboidal GS5-MOF-covered surface compared to that with a spherical GS5-NS-covered surface. (A) Experimental setup to investigate the aggregation of activated platelets in the presence of nanoparticles. (B) Representative fluorescence microscopy images and (C) quantitative fluorescence intensity data for the interaction of CFDA-SE-stained platelets (green) with Cy5-labeled CL-MOF, GS5-NS and GS5-MOF nanoparticles. (D) Representative fluorescence microscopy images and (E) quantitative fluorescence intensity data for the colocalization of CFDA-SE-stained platelets (green) and Cy5-labeled nanoparticles (red). Scale bars = 250  $\mu$ m. All images were taken at the same magnification. At least 10 images under each condition were used for analysis. (F) Schematic illustration of the measurement of the adhesion force between nanoparticles and activated platelets by AFM. (G) Typical adhesion force curves. Data are expressed as the mean  $\pm$  SD (n = 10). \*\*p < 0.01, \*\*\*p < 0.001, the abbreviation ns denotes no significant difference between the CL-MOF and GS5-NS groups.

The high Pearson's colocalization coefficient up to 0.86 of cuboidal GS5-MOFs highlights its potential of adhering stably to wound-mimicking surfaces while recruiting activated platelets to form a hemostatic plug. Cubic GS5-MOF nanoparticles showed significantly enhanced colocalization fluorescence intensity compared with spherical GS5-NS particles (**Figure 3E**), validating that the unique cubic shape of GS5-MOFs helps promote the aggregation of activated platelets.

The adhesion force between the nanoparticles and activated platelets was measured via AFM by immobilizing the nanoparticles on the cantilever and bringing them into contact with the activated platelets on the substrate (**Figure 3F**). As shown in **Figures 3G and S10**, the adhesion force values for CL-MOF, GS5-NS and GS5-MOF nanoparticles with activated platelets were 0.02, 0.11 and 0.53 nN, respectively. After GRGDS functionalization, the interaction force between the nanoparticles and activated platelets increased, while cuboidal GS5-MOF nanoparticles exhibited a greater interaction force than spherical GS5-NS particles, which implies a stronger affinity of cubic GS5-MOFs with activated platelets.

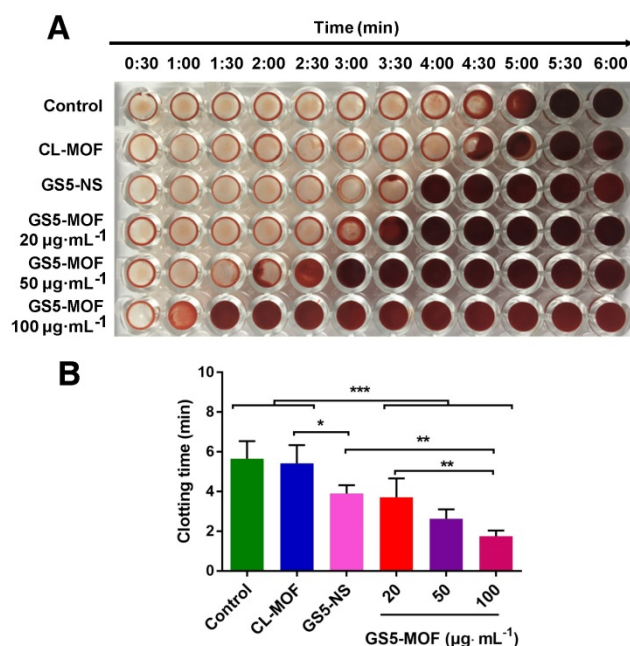


**Figure 4.** Analysis of in vitro clot formation in the presence of CL-MOF, GS5-NS and GS5-MOF nanoparticles. The cuboidal GS5-MOF nanoparticles significantly reduce the clotting time in a dose-dependent manner compared with spherical GS5-NS. (A) Images of individual wells that were washed at 30 s intervals showing the progression of clot formation. (B) Average clotting times in the presence of CL-MOF, GS5-NS and GS5-MOF nanoparticles. The results are represented as the mean  $\pm$  SD ( $n = 4-6$ ). \* $p < 0.05$ , \*\* $p < 0.01$ , \*\*\* $p < 0.001$ .

### In vitro and in vivo hemostatic effect

Based on the enhanced aggregation of activated platelets by GS5-MOF nanoparticles under static and various shear stresses, a clotting time assay was

employed to monitor clot formation time and assess the hemostatic ability in vitro [14]. **Figure 4** shows that the presence of GS5-MOF nanoparticles led to a significant decrease in the clotting time. Rat whole blood initiates coagulation in approximately 5-6 min normally and similar clotting times (5.5 min) for rat whole blood were observed in saline control wells containing no nanoparticles. The average clotting time for CL-MOFs was 5.4 min, demonstrating that CL-MOF nanoparticles had no effect on clot formation in vitro. The addition of GS5-MOF nanoparticles reduced the blood clotting time significantly in a dose-dependent manner (**Figure 4B**). The clotting times in the presence of GS5-MOFs at concentrations of 20, 50 and 100  $\mu\text{g}\cdot\text{mL}^{-1}$  was reduced by 34%, 54% and 69% respectively compared with control group. The representative images of wells (**Figure 4A**) clearly exhibit an earlier presence of a clot with the cubic GS5-MOF nanoparticles compared to their spherical counterparts. This reduced clotting time was attributed to the strong interaction of cubic GS5-MOF nanoparticles with activated platelets, which facilitates the subsequent, efficient capture of clotting factors.

To confirm the in vivo hemostatic efficiency, a mouse tail transection model was selected to investigate the capability of GS5-MOF nanoparticles to halt bleeding (**Figure 5A**). The results indicated that the normal bleeding time of a transected mouse tail was 396 s, and the blood loss was approximately 2  $\text{mL}\cdot\text{kg}^{-1}$ . Pre-injection of saline and CL-MOFs without GRGDS modification had no effect on the bleeding time or blood loss, while pre-injection of 20  $\text{mg}\cdot\text{kg}^{-1}$  GS5-MOFs resulted in a significant decrease in bleeding time to 140 s and blood loss to 0.6  $\text{mL}\cdot\text{kg}^{-1}$ , representing almost 65% reduction in bleeding time and 70% reduction in blood loss compared to saline injection (**Figures 5B and 5C**). The shortest bleeding time of 36 s and the lowest blood loss of 0.1  $\text{mL}\cdot\text{kg}^{-1}$  were achieved by injecting a high dose of GS5-MOF nanoparticles (40  $\text{mg}\cdot\text{kg}^{-1}$ ), which lowered both the bleeding time and blood loss by 90%. Subsequently, a rat femoral artery bleeding model was also employed to interrogate the hemostatic capability of GS5-MOF nanoparticles. Results revealed that the average bleeding time was 195 s when treated with saline after a femoral artery injury, whilst the bleeding time was reduced to 116 s for pre-injection of GS5-MOFs at the dose of 14  $\text{mg}\cdot\text{kg}^{-1}$ , equivalent to 20  $\text{mg}\cdot\text{kg}^{-1}$  in mouse according to body surface area. More significant hemostatic effects were achieved by increasing the dose of GS5-MOFs to 28  $\text{mg}\cdot\text{kg}^{-1}$ , which decreased the bleeding time to 79 s (**Figure 5D**). The results in rat are consistent with those observed in mouse tail transection model. Importantly, cuboidal GS5-MOF

nanoparticles possess more efficient hemostatic effects than most other reported synthetic hemostats [11,13,23,24]. For example, cholic acid and polyethylenimine formed positive nanoparticles decreased the bleeding time by 40% [13], platelet-like nanoparticles functionalized with GRGDS lowered the bleeding time in mice by 45% [24], and RGD-modified liposomes resulted in an approximately 50% reduction in bleeding time [23]. In our study, the action of spherical GS5-NS nanoparticles did not cause hemostasis as rapidly as the cuboidal-shaped GS5-MOF nanoparticles (Figures 5B, 5C and 5D), which indicated that the unique cuboidal shape plays a primary role in the efficient hemostasis of GS5-MOF nanoparticles. Interestingly, the in vivo pharmacokinetic profiles revealed that the half-life of cubic GS5-MOFs was 4.5 h, two times longer than the spherical GS5-NS (Figure 5E), indicating that cuboidal GS5-MOF nanoparticles possess a longer circulation and hemostatic effect than their spherical counterparts. These results demonstrate that introducing nonspherical carriers

such as cuboidal CL-MOF nanoparticles can lead to the development of new synthetic intravenous hemostats with high therapeutic efficacy in vivo.

Hemostasis is a balance between augmenting clotting to halt bleeding while not causing unwanted thrombosis, and any pharmacologic agent for hemostasis typically alters that balance and the risk of thrombosis is almost universally a side effect. Hence, we studied the influences of cuboidal GS5-MOF nanoparticles on coagulation function to evaluate the risk of thrombosis. Coagulation indicators such as PT, APTT, TT and FIB help doctors and researchers to accurately evaluate the coagulation status. We therefore investigated the effects of GS5-MOFs on coagulation indicators listed above. The results showed that GS5-MOFs had no effect on the coagulation function of mice and did not cause unwanted thrombosis. All the coagulation indicators were in the normal range 10 min after intravenous injection of GS5-MOF nanoparticles at the examined dose of 40 mg·kg<sup>-1</sup> (Figure 5F), and there was no significant difference with the control group,

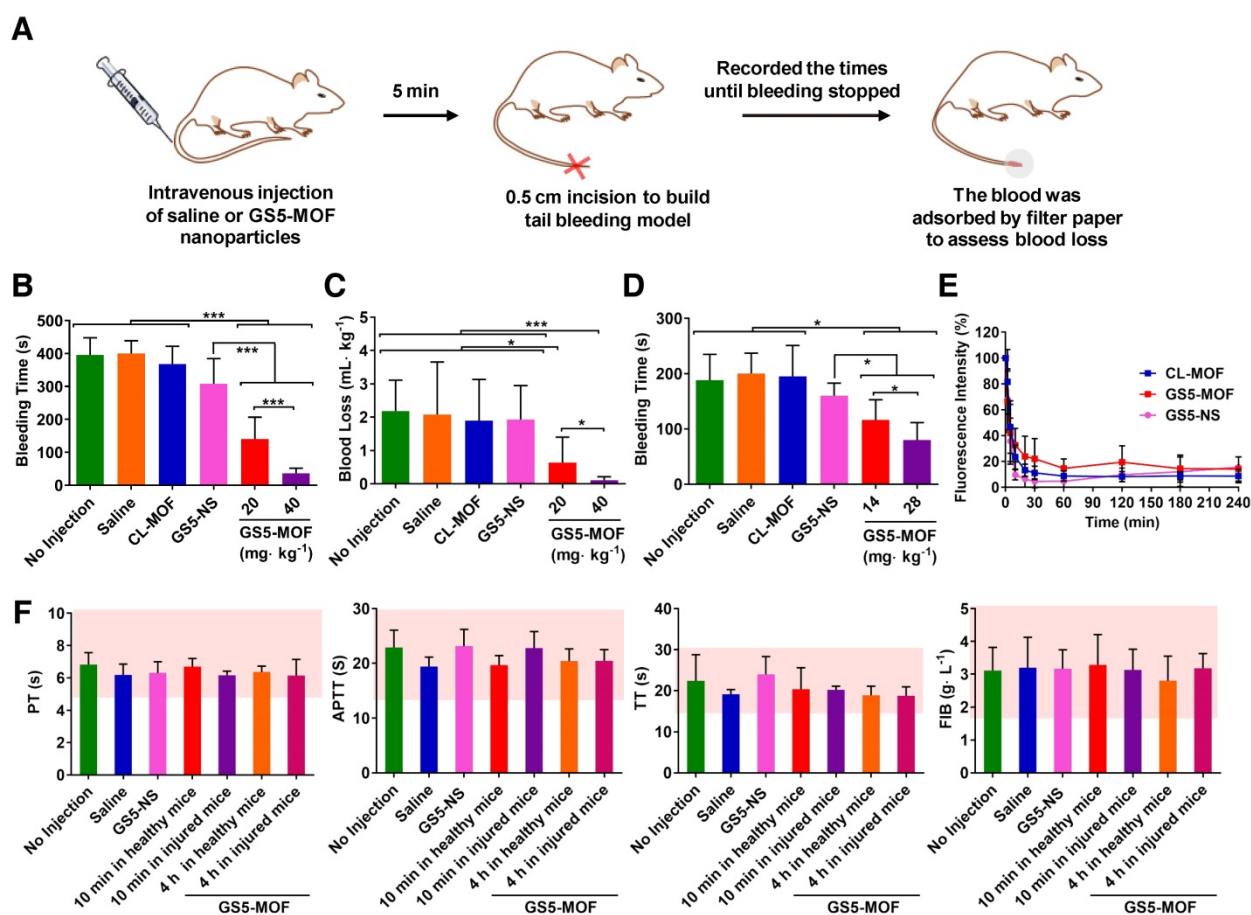


**Figure 5.** Hemostatic effects of the intravenous administration of GS5-MOF nanoparticles. The cubic-shaped GS5-MOF nanoparticles possess a more efficient hemostatic effect than spherical GS5-NS and do not trigger unwanted thrombosis. (A) Experimental schematic of the mouse tail transection assay. (B) GS5-MOF nanoparticles significantly decrease bleeding time in a mouse tail transection assay (n = 10). (C) GS5-MOF nanoparticles could reduce blood loss in a mouse tail transection assay (n = 6). (D) GS5-MOF nanoparticles significantly lower bleeding time in a rat femoral artery injury model (n = 6). (E) Pharmacokinetics of CL-MOF, GS5-MOF, and GS5-NS nanoparticles via tail vein injection in SD rats (n = 6). (F) Typical coagulation parameters of mice after injection of GS5-MOF nanoparticles at 40 mg·kg<sup>-1</sup> (n = 6). The pink windows indicate the normal levels of different parameters. Data are presented as the mean ± SD (n = 6–10). \*p < 0.05, \*\*\*p < 0.001.

indicating that the GS5-MOF nanoparticles did not affect the hemostasis balance when the blood concentration was relatively high (Figure 5E). It is interesting to note that the observed values of coagulation parameters remained within the normal range when the GS5-MOFs were cleared from the blood 4 h after treatment (Figures 5E and 5F), implying the GS5-MOFs had no long-term influence on coagulation function. To examine the potential effect of the findings for animal species dependency and increase the reliability of the results, the influences of GS5-MOFs on coagulation function in SD rats were also studied. Results showed that GS5-MOF did not cause thrombotic side effects in rats (Figure S12). These data confirm that unwanted thrombosis is not occurring when using cubic GS5-MOFs to control hemorrhage.

### In vivo targeting efficiency to vascular injuries

Platelet adhesion, activation, and subsequent aggregation at an injured site result in hemostatic plug formation after the injury. Therefore, nanoparticles that efficiently target the activated platelets at injured vessels have great potential for targeted therapy of hemorrhage, thrombosis, and atherosclerosis. To verify the activated-platelet targeting efficiency of cuboidal GS5-MOF nanoparticles in vivo, a mouse tail transection model and a mouse mesenteric thrombosis model were constructed, and the distribution of nanoparticles at the injured vascular site was evaluated by fluorescence and microCT imaging techniques.

Higher fluorescence intensity was found in the clots formed in injured mouse tail after GS5-MOFs treatment than in the clots formed after CL-MOFs and spherical GS5-NS treatment, with approximately a 4-fold and 3-fold increases, respectively (Figures 6A and 6B). The cubic GS5-MOF nanoparticles exhibited a significantly higher targeting efficiency to the activated platelets at tail clots, which is consistent with the results of in vitro platelet aggregation and in vivo hemostatic experiments. The advantageous cage-like properties of CD-MOFs enable the encapsulation of tracking agents, thus, GS5-MOF nanoparticles embedded with ultrafine silver nanoparticles (< 5 nm) were synthesized to trace the targeted deposition of GS5-MOF nanoparticles in a transected mouse tail by microCT. Importantly, Ag@CL-MOFs and Ag@GS5-MOFs are stable for 12 h, which ensures that silver nanoparticles would not escape from the Ag@CL-MOFs and Ag@GS5-MOFs during the targeting experiment. In axial and sagittal microCT slices, the gray value for the silver signal concentrated in the mouse tail clot was between 20000 and 30000, while the gray value in peripheral tissues

was below 20000, which allowed accurate identification of Ag@CL-MOFs and Ag@GS5-MOFs in the mouse tail transection (Figures 6C and S13). Furthermore, the silver content was also confirmed via inductively coupled plasma mass spectrometry (ICP-MS) (Table S4). The strong silver signal in the damaged mouse tail demonstrated the specific targeting and accumulation of GS5-MOF nanoparticles at the injured vessels. Unfortunately, the microCT experiment could not be carried out with GS5-NS particles due to the lack of ordered cavity in CD-NS. Furthermore, the microCT experiment highlighted that Ag@GS5-MOF nanoparticles can be used as a microCT contrast agent for the direct imaging of vascular injury-related diseases.

For the mouse mesenteric thrombosis model, the fluorescent dye rhodamine B was used to visualize FeCl<sub>3</sub>-treated mesenteric artery/vein thrombus. A large number of platelets were recruited and activated to the obstructed blood vessels (Figure 6D). The cubic GS5-MOF nanoparticles target and accumulate at thrombus sites, with a Pearson's coefficient of approximately 0.65, which was significantly higher than that of spherical GS5-NS nanoparticles (Figure 6E). These findings indicate that the in vivo targeting to injured vessels is dependent on the shape of the nanoparticle, the cuboidal GS5-MOF nanoparticles have superior targeting efficiency compared to spherical counterpart and possess great potential to deliver therapeutic drugs specifically to the bleeding site or thrombus.

### Conclusions

Different from particles with conventional shapes such as spheres, unique cuboidal nanoparticles with uniform size and ordered cyclodextrin frameworks were verified to achieve higher hemostasis and injured vessels targeting compared to spherical counterpart. By tethering the ordered  $\gamma$ -CDs in CD-MOFs via crosslinking and modifying the surface with GRGDS peptide, GS5-MOF nanoparticles significantly promote the aggregation of activated platelets in vitro, markedly reduced both the bleeding time and blood loss by 90% in mice. More importantly, the studies demonstrate that the cuboidal GS5-MOF nanoparticles target and accumulate at the injured vessels in a mouse tail transection bleeding model and a mouse mesenteric thrombosis model, significantly superior to spherical  $\gamma$ -CD nanospoges with identical chemical compositions. Results confirm the critical role of nanoparticle shapes in achieving control of hemorrhage. Cubic GS5-MOFs have been shown to target activated platelets more efficiently and have higher local concentration at the injured walls under

flow than spherical counterpart. Whilst mechanistic understanding of this effect remains to be fully revealed, the cuboidal nanoparticles may function as supramolecular cross-linkers to augment platelet

aggregation and hemostasis by increasing the collision frequency and contact surface area with activated platelets.

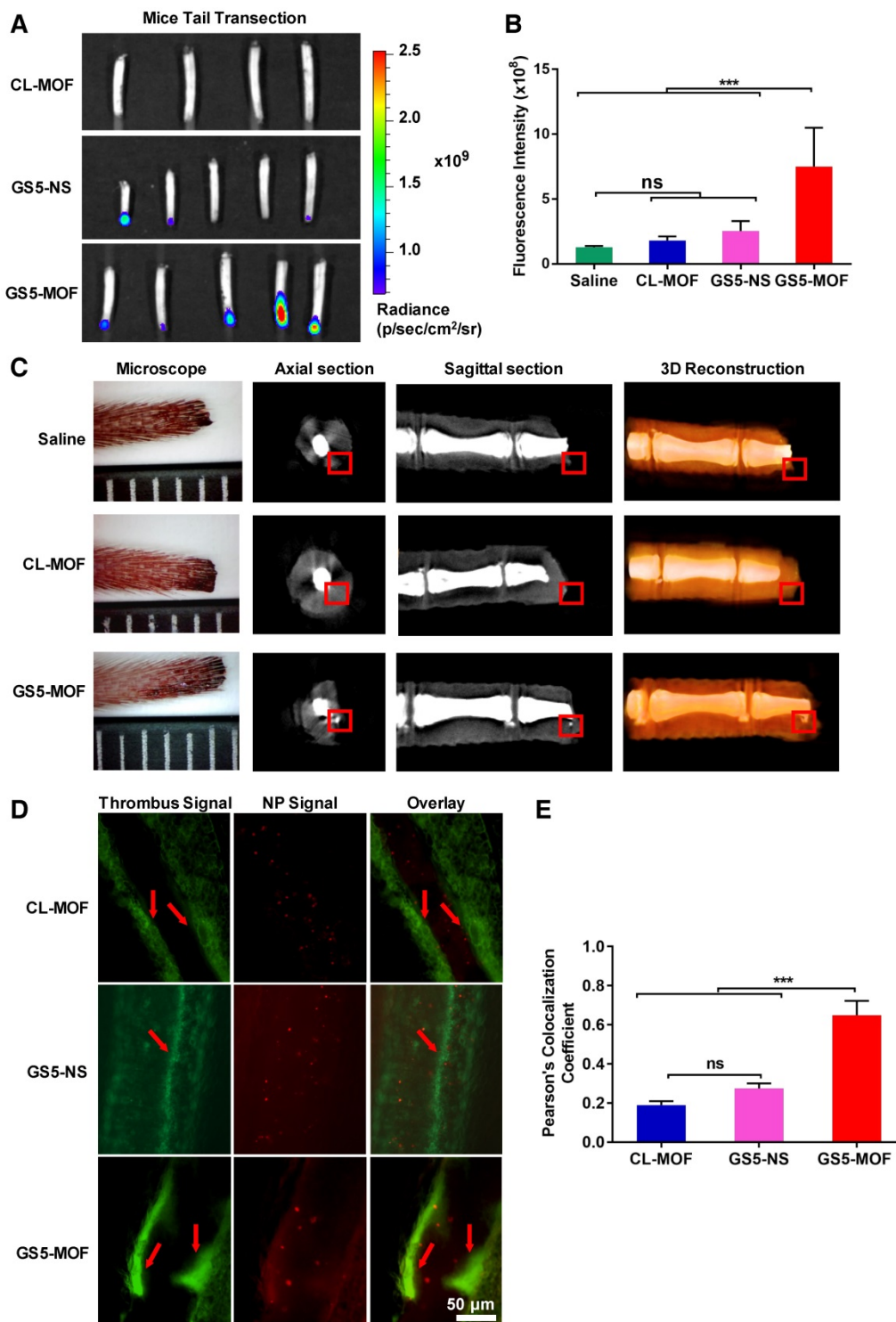


**Figure 6.** In vivo targeting efficiency of GS5-MOF nanoparticles to vascular injuries in a mouse tail transection model and a mouse mesenteric thrombosis model. The cuboidal GS5-MOF nanoparticles exhibit significantly higher targeting capacity for damaged vascular sites. (A) Representative fluorescence images of transected mouse tails after intravenous injection of nanoparticles confirmed that fluorescently labeled GS5-MOF nanoparticles targeted at the tail-section clot. (B) Quantification of the fluorescence intensity in the transected tails. (C) MicroCT axial slice, sagittal slice and 3D-reconstruction images of mouse tail transection after injection of Ag@CL-MOF and Ag@GS5-MOF nanoparticles. The red rectangles indicate the silver signal. The smallest division of the ruler is 1 mm. (D) Representative fluorescence images of mouse mesenteric thrombosis induced by FeCl<sub>3</sub>, and the inserted arrow shows the formation of thrombus with higher fluorescence intensity. Scale bar = 50  $\mu$ m. (E) Quantitative fluorescence intensity data for the colocalization of rhodamine B labeled activated platelets (green) and Cy5-labeled nanoparticles (red). All images were taken at the same magnification. Data are expressed as the mean  $\pm$  SD (n = 4-5). \*\*\*p < 0.001, the abbreviation ns denotes no significant difference between groups.

In considering the potential of these agents as novel drug delivery systems, it is interesting to note that the CD-MOFs used in this study are composed of materials with proven biocompatibility and pharmaceutically approved excipients ( $\gamma$ -CD). CD-MOFs are also highly porous containing spherical pores of 1.7 nm in diameter with  $\gamma$ -CD tori of 0.78 nm across, both of which can accommodate active drug molecules, imaging agents or co-deliver theranostic agents. Active substances have been loaded and delivered by CD-MOF related materials successfully [35,43], and diagnostic agent such as silver nanoparticles were embedded into GS5-MOFs for microCT imaging in our study. The cuboidal tethered GS5-MOF nanoparticles show great potential to deliver drugs and imaging agents for efficient diagnosis and targeted therapy of vascular diseases. In summary, cuboidal cyclodextrin frameworks not only can be used as an injectable hemostat to control incompressible wounds but also possess great potential for targeted vascular delivery to treat various vascular disorders including cancer, thrombosis, and hemorrhage and inflammation. Our findings demonstrate the key role of nanoparticle shape on achieving hemostasis and in vivo targeting, and provide a basis for designing novel, effective drug delivery systems.

## Abbreviations

ADP: adenosine 5' -diphosphate; AFM: atomic force microscopy measurements; Ag@CD-MOFs: Ag-loaded CD-MOFs; Ag@CL-MOFs: Ag-loaded CL-MOFs; Ag@GS5-MOFs: Ag-loaded GS5-MOFs; APTT: activated partial thromboplastin time; BSA: bovine serum albumin; CDI: N,N'-carbonyldiimidazole; CD-MOFs:  $\gamma$ -cyclodextrin metal-organic frameworks; CD-NS:  $\gamma$ -cyclodextrin nanosponges; CFDA-SE: carboxyfluorescein diacetate succinimidyl ester; CL-MOFs: crosslinked CD-MOFs; Cy5: cyanine 5 NHS ester; DLS: dynamic light scattering; DMAP: 4-dimethylaminopyridine; DMF: N,N-dimethylformamide; DMSO: dimethyl sulfoxide; DPC: diphenyl carbonate; EDC: 1-(3-Dimethylaminopropyl)-3-ethylcarbodiimide; FIB: fibrinogen content; FTIR: Fourier transform infrared; GRGDS: Gly-Arg-Gly-Asp-Ser; GS5-MOFs: CL-MOFs modified with GRGDS peptide; GS5-NS: CD-NS nanoparticles modified with GRGDS peptide;  $^1\text{H}$  NMR:  $^1\text{H}$  nuclear magnetic resonance; ICP-MS: inductively coupled plasma mass spectrometry; IVIS: in vivo imaging system; KOH: potassium hydroxide; MOFs: metal-organic frameworks; PBS: phosphate buffer; PEG 20000: polyethylene glycol 20000; PLNs: platelet-like nanoparticles; PLPs: platelet-like particles; PPEC: parallel plate flow chamber; PPP:

platelet-poor plasma; PRP: platelet-rich plasma; PT: prothrombin time; SD rats: Sprague-Dawley rats; SEM: scanning electron microscopy; SSRF: shanghai synchrotron radiation facility; TEA: triethylamine; TFE: 2,2,2-trifluoroethanol; TT: thrombin time.

## Supplementary Material

Supplementary methods, figures and tables.  
<http://www.thno.org/v09p2489s1.pdf>

## Acknowledgements

The authors are thankful to the financial support from the Strategic Priority Research Program of the Chinese Academy of Sciences (XDA12050307); Key Program for International Science and Technology Cooperation Projects of China (2016YFE0125100); Research Foundation of the Shanghai Institute of Materia Medica (CASIMM0120182001) and National Natural Science Foundation of China (81573392 and 81430087).

## Authorship

Y. He, J. Xu and X. Sun performed research, J. Zhang, Y. Su and H. Li designed research, P. York and A. Maharjan contributed to the microCT test, X. Ren and Y. He analyzed data, Y. He and all prepared the manuscript.

## Competing Interests

The authors have declared that no competing interest exists.

## References

- Calin M, Manduteanu I. Emerging nanocarriers-based approaches to diagnose and reduce vascular inflammation in atherosclerosis. *Curr Med Chem.* 2017; 24: 550-67.
- Kelley WJ, Safari H, Lopez-Cazares G, Eniola-Adefeso O. Vascular-targeted nanocarriers: design considerations and strategies for successful treatment of atherosclerosis and other vascular diseases. *Wiley Interdiscip Rev Nanomed Nanobiotechnol.* 2016; 8: 909-26.
- Modery-Pawlowski CL, Li W, Sun M, Ravichandran K, Hickman D, Kos C, et al. Platelet microparticle-inspired clot-responsive nanomedicine for targeted fibrinolysis. *Biomaterials.* 2017; 128: 94-108.
- Geng Y, Dalhaimer P, Cai S, Tsai R, Tewari M, Minko T, et al. Shape effects of filaments versus spherical particles in flow and drug delivery. *Nat Nanotechnol.* 2007; 2: 249-55.
- Yu M, Wang J, Yang Y, Zhu C, Su Q, Guo S, et al. Rotation-facilitated rapid transport of nanorods in mucosal tissues. *Nano Lett.* 2016; 16: 7176-82.
- Behrens AM, Sikorski MJ, Kofinas P. Hemostatic strategies for traumatic and surgical bleeding. *J Biomed Mater Res A.* 2014; 102: 4182-94.
- Champion HR, Bellamy RF, Roberts CP, Leppaniemi A. A profile of combat injury. *J Trauma.* 2003; 54 (Suppl): S13-9.
- Cloonan CC. Treating traumatic bleeding in a combat setting: possible role of recombinant activated factor VII. *Mil Med.* 2004; 169: 16-8.
- Hickman DA, Modery-Pawlowski CL, Sekhon UDS, Marks J, Sen Gupta A. Biomaterials and advanced technologies for hemostatic management of bleeding. *Adv Mater.* 2018; 30: 1700859.
- Chan LWG, White NJ, Pun SH. Synthetic strategies for engineering intravenous hemostats. *Bioconjug Chem.* 2015; 26: 1224-36.
- Bertram JP, Williams CA, Robinson R, Segal SS, Flynn NT, Lavik EB. Intravenous hemostat: nanotechnology to halt bleeding. *Sci Transl Med.* 2009; 1: 11ra22.
- Long M, Zhang Y, Huang P, Chang S, Hu Y, Yang Q. Emerging nanoclay composite for effective hemostasis. *Adv Funct Mater.* 2018; 28: 1704452.
- Cheng J, Feng S, Han S, Zhang X, Chen Y, Zhou X, et al. Facile assembly of cost-effective and locally applicable or injectable nanohemostats for hemorrhage control. *ACS Nano.* 2016; 10: 9957-73.

14. Gaharwar AK, Avery RK, Assmann A, Paul A, McKinley GH, Khademhosseini A, et al. Shear-thinning nanocomposite hydrogels for the treatment of hemorrhage. *ACS Nano*. 2014; 8: 9833-42.
15. Lashof-Sullivan MM, Shoffstall E, Atkins KT, Keane N, Bir C, VandeVord P, et al. Intravenously administered nanoparticles increase survival following blast trauma. *Proc Natl Acad Sci U S A*. 2014; 111: 10293-8.
16. Hansen CE, Myers DR, Baldwin WH, Sakurai Y, Meeks SL, Lyon LA, et al. Platelet-microcapsule hybrids leverage contractile force for targeted delivery of hemostatic agents. *ACS Nano*. 2017; 11: 5579-89.
17. Qin X, Labuda K, Chen J, Hruschka V, Khadem A, Liska R. Development of synthetic platelet-activating hydrogel matrices to induce local hemostasis. *Adv Funct Mater*. 2016; 25: 6606-17.
18. Modery-Pawłowski CL, Kuo HH, Baldwin WM, Sen Gupta A. A Platelet-inspired paradigm for nanomedicine targeted to multiple diseases. *Nanomedicine (Lond)*. 2013; 8: 1709-27.
19. Modery-Pawłowski CL, Tian LL, Pan V, McCrae KR, Mitragotri S, Sen Gupta A. Approaches to synthetic platelet analogs. *Biomaterials*. 2013; 34: 526-41.
20. Ravikumar M, Modery-Pawłowski CL, Wong TL, Dzuricky M, Sen Gupta A. Mimicking adhesive functionalities of blood platelets using ligand-decorated liposomes. *Bioconjug Chem*. 2012; 23: 1266-75.
21. Okamura Y, Fujie T, Nogawa M, Maruyama H, Handa M, Ikeda Y, et al. Haemostatic effects of polymerized albumin particles carrying fibrinogen  $\gamma$ -chain dodecapeptide as platelet substitutes in severely thrombocytopenic rabbits. *Transfus Med*. 2008; 18: 158-66.
22. Modery-Pawłowski CL, Ravikumar M, Wong TL, Dzuricky MJ, Durongkaveroj N, Sen Gupta A. Heteromultivalent liposomal nanoconstructs for enhanced targeting and shear-stable binding to active platelets for site-selective vascular drug delivery. *Biomaterials*. 2011; 32: 9504-14.
23. Modery-Pawłowski CL, Tian LL, Ravikumar M, Wong TL, Sen Gupta A. In vitro and in vivo hemostatic capabilities of a functionally integrated platelet-mimetic liposomal nanoconstruct. *Biomaterials*. 2013; 34: 3031-41.
24. Anselmo AC, Modery-Pawłowski CL, Menegatti S, Kumar S, Vogus DR, Tian LL, et al. Platelet-like nanoparticles: mimicking shape, flexibility, and surface biology of platelets to target vascular injuries. *ACS Nano*. 2014; 8: 11243-53.
25. Doshi N, Prabhakarandian B, Rearmsey A, Pant K, Sundaram S, Mitragotri S. Flow and adhesion of drug carriers in blood vessels depend on their shape: a study using model synthetic microvascular networks. *J Control Release*. 2010; 146: 196-200.
26. Tao L, Hu W, Liu Y, Huang G, Sumer BD, Gao J. Shape-specific polymeric nanomedicine: emerging opportunities and challenges. *Exp Biol Med (Maywood)*. 2011; 236: 20-9.
27. Brown AC, Stabenfeldt SE, Ahn B, Hannan RT, Dhada KS, Herman ES, et al. Ultrasoft microgels displaying emergent platelet-like behaviours. *Nat Mater*. 2014; 13: 1108-14.
28. Toy R, Hayden E, Shoup C, Baskaran H, Karathanasis E. The effects of particle size, density and shape on margination of nanoparticles in microcirculation. *Nanotechnology*. 2011; 22: 115101.
29. Pillai JD, Dunn SS, Napier ME, DeSimone JM. Novel platforms for vascular carriers with controlled geometry. *IUBMB Life*. 2011; 63: 596-606.
30. Luo Z, Fan S, Gu C, Liu W, Li B, Liu J. Metal-organic framework (MOF)-based nanomaterials for biomedical applications. *Curr Med Chem*. 2018; 25.
31. Wu MX, Yang YW. Metal-organic framework (MOF)-based drug/cargo delivery and cancer therapy. *Adv Mater*. 2017; 29: 1606134.
32. Cai W, Chu CC, Liu G, Wang YX. Metal-organic framework-based nanomedicine platforms for drug delivery and molecular imaging. *Small*. 2015; 11: 4806-22.
33. Deshayes S, Gref R. Synthetic and bioinspired cage nanoparticles for drug delivery. *Nanomedicine (Lond)*. 2014; 9: 1545-64.
34. Della Rocca J, Liu D, Lin W. Nanoscale metal-organic frameworks for biomedical imaging and drug delivery. *Acc Chem Res*. 2011; 44: 957-68.
35. Li H, Lv N, Li X, Liu B, Feng J, Ren X, et al. Composite CD-MOF nanocrystals-containing microspheres for sustained drug delivery. *Nanoscale*. 2017; 9: 7454-63.
36. Shende P, Kulkarni YA, Gaud RS, Deshmukh K, Cavalli R, Trotta F, et al. Acute and repeated dose toxicity studies of different  $\beta$ -cyclodextrin-based nanosponge formulations. *J Pharm Sci*. 2015; 104: 1856-63.
37. Caldera F, Tannous M, Cavalli R, Zanetti M, Trotta F. Evolution of cyclodextrin nanosponges. *Int J Pharm*. 2017; 531: 470-9.
38. Liu B, Li H, Xu X, Li X, Lv N, Singha V, et al. Optimized synthesis and crystalline stability of  $\gamma$ -cyclodextrin metal-organic frameworks for drug adsorption. *Int J Pharm*. 2016; 514: 212-9.
39. Singh V, Guo T, Wu L, Xu J, Liu B, Gref R, et al. Template-directed synthesis of a cubic cyclodextrin polymer with aligned channels and enhanced drug payload. *RSC Adv*. 2017; 7: 20789-94.
40. Nguyen TH, Palankar R, Bui VC, Medvedev N, Greinacher A, Delcea M. Rupture forces among human blood platelets at different degrees of activation. *Sci Rep*. 2016; 6: 25402.
41. Wei Y, Han S, Walker DA, Fuller PE, Grzybowski BA. Nanoparticle core/shell architectures within MOF crystals synthesized by reaction diffusion. *Angew Chem Int Ed Engl*. 2012; 51: 7435-9.
42. Li W, Nieman M, Sen Gupta A. Ferric chloride-induced murine thrombosis models. *J Vis Exp*. 2016; 115: e54479.
43. Singh V, Guo T, Xu H, Wu L, Gu J, Wu C, et al. Moisture resistant and biofriendly CD-MOF nanoparticles obtained via cholesterol shielding. *Chem Commun*. 2017; 53: 9246-9.